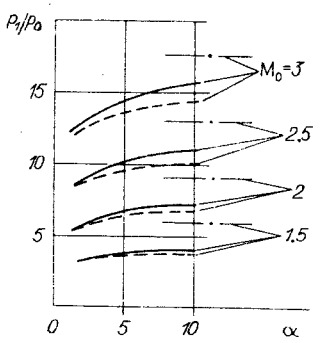

Fig. 2

As in the previous case, we can show that the (M_0, λ_*) segment in (8) has a single root for $M_0 > 1$. Therefore, the root in (7) or (8) is localized and there is no difficulty in finding λ in each of the cases.

Figure 2 shows the α dependence of the pressure increase p_1/p_0. The solid lines correspond to a bulk source and the dashed ones to a mass one. The horizontal lines denote the levels at which the curves flatten off for infinite heat production.

The results obtained directly from the solution agree very well with numerical calculations from the nonstationary gas-dynamic equations.

LITERATURE CITED

1. G. A. Abramovich, Applied Gas Dynamics [in Russian], Nauka, Moscow (1969).
2. F. Barthlemy, Combustion Gas Dynamics [Russian translation], Énergoizdat, Moscow (1981).
3. K. P. Stanyukovich, Nonstationary Motion in a Continuous Medium [in Russian], Nauka, Moscow (1971).
4. L. V. Ovsyannikov, Lectures on Gas-Dynamic Principles [in Russian], Nauka, Moscow (1981).

SHEAR INTERFEROMETRY APPLIED TO THE DENSITY DISTRIBUTION IN A LAMINAR BOUNDARY LAYER

D. A. Van, A. A. Maslov, and A. L. Rudnitskii

UDC 535:532.526

The theoretical models used for laminar supersonic boundary layers have not been tested by experiment because of the limitations in classical measurement methods. Pneumometric methods employ sensors whose sizes are comparable with the boundary-layer thickness (that thickness is not more than 1 mm in supersonic wind tunnels). Thermoanemometers give good resolution but the characteristics alter in the transonic region, which makes them difficult to use. Also, the sensor may distort the boundary layer.

Indirect methods are used in measuring density, temperature, and velocity profiles for supersonic flows; these methods require additional assumptions and empirical constants to give quantitative results. Optical methods enable one to measure density profiles without perturbing the flow. The spatial resolution in an interference method is restricted to $d = 1.6\sqrt{\lambda L}$ (λ wavelength and L size along the beam), which means that a flat object 200 mm wide allows one to obtain independent readings with a step of 0.5 mm [1]. The resolution can be increased by one or two orders of magnitude on a cylindrical object, but then the total phase shift along the beam in the laminar layer becomes comparable with the usual sensitivity of 0.05-0.1 λ. The sensitivity is limited by the accuracy in determining the turning points,

Novosibirsk. Translated from Zhurnal Prikladnoi Mekhaniki i Tekhnicheskoi Fiziki, No. 3, pp. 62-66, May-June, 1988. Original article submitted February 11, 1987.

0021-8944/88/2903-0369$12.50

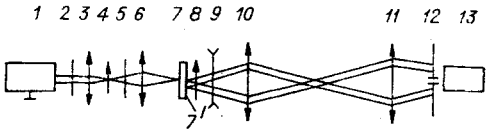

Fig. 1

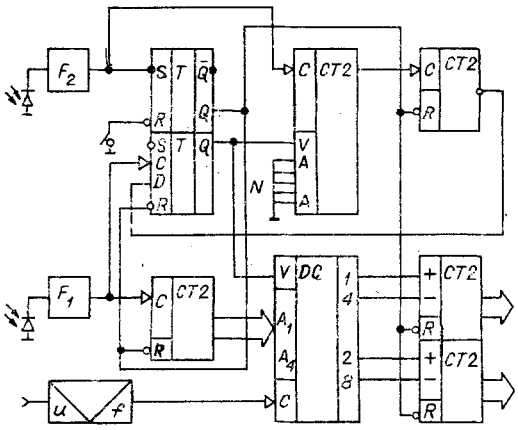

Fig. 2

which are usually unevenly placed. An alternative method of determining the density distribution in a stationary pattern is to scan the field with a focussed laser beam [1].

The Institute of Theoretical and Applied Mechanics, Siberian Division, USSR Academy of Sciences, has developed a scanning shear interferometer based on focussed beams and photoelectric recording, which enables one to measure the density profile in the convective boundary layer at the lower surface of a horizontal heated cylinder or on the laminar boundary layer around a cone in the supersonic flow with a spatial resolution of 30 μm and sensitivity 10^{-3} λ. A similar method has been used to measure radial refractive-index distributions in glass fibers with a spatial resolution of about 2 μm.

The interferometer (Fig. 1) consists of the light source 1, which is a standard He–Ne laser with Lamb-dip stabilization, output 0.5 mW, together with two quarter-wave plates 2 and 5, the focussing lenses 3, 6, 10, and 11, the birefringent plate 7, polaroids 4 and 8 (4 attached to the shaft of a synchronous motor), the optical scanning device 9, photocell 13, and inlet slit 12. The shaping device consists of the two quarter-wave plates, the lenses 3 and 6, the polaroid 4, and the birefringent plate in the plane 7', which produce two coherent point sources having complementary planes of polarization, whose frequencies differ from each other by twice the polaroid rotation frequency 2Ω. The beams from these sources are focussed by lens 10 in the working region and then interfere. Polaroid 8 has its plane of polarization at $\pi/4$ to the planes of the point sources, which enables one to view the interference pattern in the plane of the slit in front of the photocell. The fringes move with respect to the slit in such a way that the output is a sinusoidal signal having frequency 2Ω, whose phase is related to the angle of rotation in polaroid 4. The additional optical path difference δ between the beams is due to change in the refractive index (density) and causes an additional phase shift.

The scanning device 9 is located in the front focal plane of the lens 10 and consists of a lens and micrometer screw, which provide parallel displacement for the focussed beams within the aperture of lens 10 (in particular, transverse to the boundary layer).

The additional phase difference at any point r is

$$\Delta\varphi(r) = \varphi(r) - \varphi(r + a) \tag{1}$$

or

$$\Delta\varphi(r) = \int_{r}^{r+a} (\partial\varphi/\partial x)\, dx, \tag{2}$$

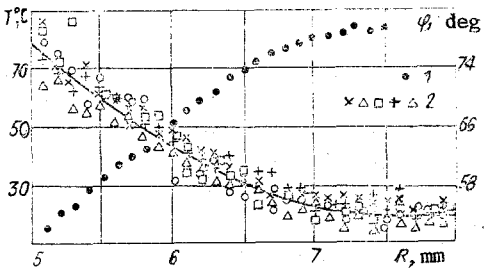

Fig. 3

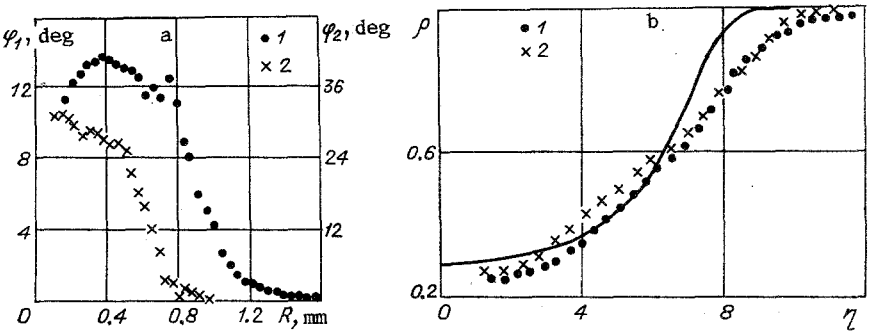

Fig. 4

where a is the baseline and $\partial\varphi/\partial x$ is the projection of the gradient in the phase distribution $\varphi(r)$ on a.

To a first approximation, the measured shifts $\Delta\varphi(r)$ are proportional to $\partial\varphi/\partial x$, so such an interferometer is often called differential, including in the panoramic case [2]. In that approximation, the spatial resolution along the x axis is equal to the baseline. It has been shown [3] that the sensitivity is the same in measuring the density gradient in this way as it is in schlieren measurements from the deflection of a Gaussian beam if the spatial resolution is the same.

However, one can solve (1) to derive $\varphi(r)$ with a resolution limited only by the diffraction. The uncertainty relation is $d\theta \geqslant \lambda/\pi$ (d beam diameter at the focus and θ aperture, with the diameter and aperture for a Gaussian beam determined at the e^{-2} intensity level). Gaussian beams (laser zero transverse modes) have a minimality feature, and this relation is obeyed exactly for them. When one examines a three-dimensional object having parameter L, the resolution is limited on the one hand by the minimal diameter at the focus and on the other by the beam size at the edge of the object, which is proportional to $\theta L/2$. The resolution is $d = 1.6\sqrt{\lambda L}$ when these parameters are chosen optimally.

The recording device has simple quasioptimal signal accumulation in two reversible counters (Fig. 2, standard symbols). The sinusoidal signal passes to a linear voltage-frequency converter, which gives a pulse train whose frequency at any instant is proportional to the input voltage. The pulses pass through the decoder DC and are summed in turn by the reversible binary counters CT2, where the reset pulse R sets them to zero at the start of each measurement cycle. The outputs from DC are switched by the synchronizing pulses provided by the shaper F_1 placed near the rotating polaroid 4 in such a way that the signal in each period produces four synchronizing pulses. The other shaper F_2 produces a single pulse on a rotation of polaroid 7, which is used for triggering the recording device and strobing DC after a given number of periods by means of two D flip-flops T and the two binary counters CT2. Usually, the signal accumulation time is about 1 sec.

Summing the signals with the reversible counters in each channel is equivalent to integrating the signal in the corresponding quarter periods. The phase is deduced from $\varphi = \mathrm{Arctg}\,(I_1/I_2)$, where I_1 and I_2 are the counter readings. It can be shown that this algorithm provides quasioptimal phase measurement with a standard deviation 1.2 times the optimal value if there is additive noise; if there is multiplicative noise, the performance is worse by a factor two.

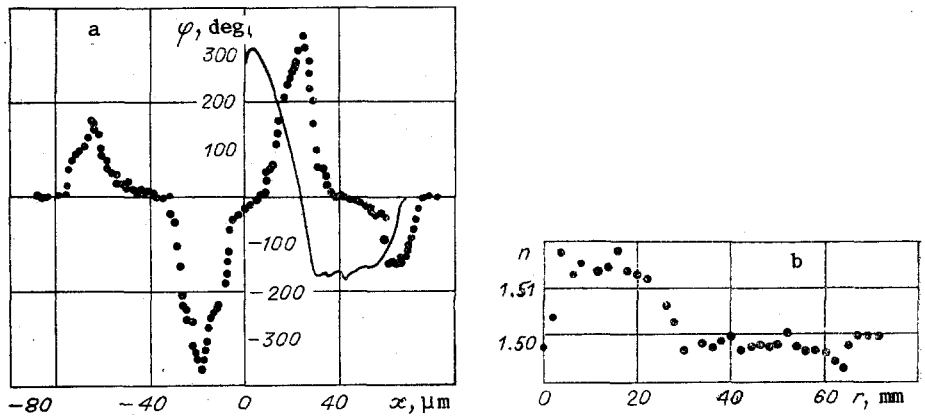

Fig. 5

With a 1-sec accumulation time, the standard deviation was 0.05° or 10^{-4} λ, which corresponds to a shift of 0.1 nm. In measurements with prototypes, the standard deviation was 0.5-1.2° and was determined in the main by the high vibrational level in the working area around the wind tunnel, as well as by instability in the convective boundary layer, while in measurements on glass fibers, it was governed by the accuracy in positioning the fiber relative to the beams of ±0.5 μm and thus was about 10°.

The measurements gave the density (refractive index) distribution, where the Abel equation was solved by piecewise-parabolic interpolation applied to the measurements at several points. As the phase shifts are proportional to $\partial\varphi/\partial x$ in the first approximation, and this appears in the inverse Abel transformation, the solution is more stable than that for an ordinary Abel equation.

The points 1 in Fig. 3 show the phase shifts φ(R), where R is radial distance, in a convective boundary layer around a horizontal cylinder 10 mm in diameter. The cylinder was an aluminum tube carrying water at 78°C. The baseline was 0.4 mm, and beam diameter, 50 μm. The tube was mounted in a stand and was moved vertically with a micrometer. The temperature distribution (line in Fig. 3) calculated from the density distribution was compared with direct temeprature measurements made with a copper-constantan thermocouple having wires 20 μm in diameter and 50 μm junction (points 2). The thermocouple wires were parallel to the generator in order to eliminate heat leak along them.

Density profiles were measured in a laminar boundary layer on a cone in a supersonic wind tunnel at this institute, type T-325 [4], where the working part was 200 × 200 mm in size and the Mach number in the unperturbed flow was M = 4. The flow parameters (forechamber temperature, static pressure in the working part, and total pressure in the forechamber) were determined with apparatus standard for wind tunnels. The cone was made of ebonite to eliminate heat transfer with the boundary layer. The length was 335 mm, base diameter, 50 mm, and angle at vertex, 10°. The point was blunted to a radius of about 0.2 mm. The model was set up at the center of the working part at zero angle of attrack.

The measurements were made with x = 138 and 130 mm (x is the distance from the point to the position of measurement). The measured pressure in the forechamber in the first case gave the Reynolds number $\mathrm{Re} = ux/\nu$ as 1.07×10^6, while in the second it was 1.8×10^6 (u and ν are the velocity and viscosity at the edge of the boundary layer). The baselines were 0.2 and 0.37 mm and beam diameter, 30 μm. The beams were positioned with an accuracy of 10 μm, and with the wind tunnel working, the noise level was 110-120 dB and the vibrational level was high, but the fluctuations in the position had an amplitude not more than 5 μm. The model position was not monitored.

Parts a and b in Fig. 4 show the measured phase shifts and the dimensionless density profiles calculated from them, where points 1 and 2 correspond to Re of 1.8×10^6 and 1.07×10^6, ρ is the density referred to that at the edge of the boundary layer, and $\eta = (y/x)\sqrt{3ux/2\nu}$ is the dimensionless Blasius coordinate referred to a flat plate. The line showing the dimensionless density profile has been derived by numerical integration applied to the boundary-layer equations for a gradient-free flow on a plate. In the calculations, the Prandtl

number was $\sigma = 0.72$, adiabatic parameter $\gamma = 1.41$, and Sutherland's temperature dependence of the viscosity was used, with $\eta = (y/x)\sqrt{ux/2\nu}$. One can then make a direct comparison because the boundary layers on a plate and cone coincide if the transverse dimensions are in the relation $\sqrt{3}$. $M_\delta = 3.8$ at the outer edge of the boundary layer. The dimensionless density profiles coincide satisfactorily one with another and with the calculations, but the thickness is 20% larger than the calculated value. The observed profiles are also different in shape.

To reduce the refraction at the boundaries of a glass fiber, the latter was placed in glycerol between two plane-parallel glass plates, and this assembly was mounted on an optical stage having micrometer adjustments, and scale division was 1 μm. The focussing lens (10 in Fig. 1) was a ×10 microscope objective. The visible beam diameter was 2 μm, while the baseline was 12 μm. Figures 5, a and b, show the measured phase shifts as points and calculations on the radial refractive-index distributions. The line in Fig. 5a is the total phase shift along the chord of the fiber calculated from the measurements.

This interferometer with focussed beams and photoelectric recording is effectively a schlieren instrument with digital readout at any point on the object (including points in a uniform grid) with a spatial resolution limited only by diffraction and a sensitivity of 0.1-1°. The instrument can be used on wind tunnels and other systems having high vibrational levels.

Independent measurements are required to establish why the laminar boundary layer is wider than the calculated value; this would be simplest to do by means of some local optical method such as Rayleigh scattering [5] or Raman scattering [6]. It is also necessary to monitor the model position stability.

LITERATURE CITED

1. A. L. Rudnitskii, "Differential optical measurements on gas-flow parameters", Modern Methods of Examining Heat and Mass Transfer [in Russian], ITMO AN BSSR, Minsk (1981), Part 1.
2. D. Malakary (ed.), Optical Process Monitoring [Russian translation], Mashinostroenie, Moscow (1985).
3. A. L. Rudnitskii, Developments in Optical Methods of Examining Gas Flows and Plasmas: Ph. D. Thesis [in Russian], ITPM SO AN SSSR, Novosibirsk (1985).
4. G. I. Bagaev, V. A. Lebiga, V. G. Pridanov, and V. V. Chernykh, "The T-325 supersonic wind tunnel with reduced turbulence", Aerophysical Researches [in Russian], ITPM SO AN SSSR, Novosibirsk (1972).
5. R. W. Pitz, R. Cattolica, et al., "Temperature and density in hydrogen–air flame from Rayleigh scattering", Combust. Flame, 27, No. 3 (1976).
6. A. L. Rudnitskii, S. Yu. Fedorov, and Yu. A. Yakobi, "A coherent Raman-scattering spectrometer based on intracavity scattering", Optical Methods of Examining Gas Flows and Plasmas [in Russian], ITMO AN BSSR, Minsk (1982).